Effect of Torrefaction Temperature and O_2 Concentration on the Pyrolysis Behaviour of Moso Bamboo

Yi Sun,[a,b] Yuquan Sun,[b] Wei Chen,[b] Shanshan Wang,[a] Guangyuan Liang,[a] Wenzhu Li,[a] Zhongqing Ma,[a,*] and Wenbiao Zhang [a,*]

Five-year-old moso bamboo was torrefied under nitrogen and different oxygen concentrations of 3% to 9% and torrefaction temperatures of 200 °C to 300 °C. Mass yields of 31.7% to 96.6%, energy yields of 30.8% to 98.9%, and higher heating values (HHVs) in the range 18.8 to 27.1 MJ/kg were obtained. The torrefied sample was characterized by Fourier transform infrared spectrometry (FTIR). Under the different torrefaction temperatures and oxygen concentrations, hemicellulose and cellulose were thermally decomposed, which led to significant changes in the chemical functional groups of the raw and torrefied bamboo. The pyrolysis experiments on raw and torrefied bamboo were conducted using the pyrolyzer coupled with a gas chromatography/mass spectrometer (Py-GC/MS). According to the Py-GC/MS analysis, the pyrolytic bio-oil were mainly composed of acids, furans, phenols, ketones, aldehydes, esters, alcohols, and hydrocarbons. Higher torrefaction temperature reduced the relative contents of acids, ketones, furans, and aldehydes. However, lower torrefaction temperatures and moderate oxygen concentrations were optimal for the production of phenols and hydrocarbons.

Keywords: Biomass; Oxygen torrefaction; Oxygen concentration; Fast pyrolysis

*Contact information: a: School of Engineering, Zhejiang Provincial Collaborative Innovation Center for Bamboo Resources and High-Efficiency Utilization, Zhejiang A & F University, Hangzhou, Zhejiang 311300, China; b: Shangdong Institute for Product Quality Inspection, Jinan, Shandong 250102, China; * Corresponding authors: zwb@zafu.edu.cn*

INTRODUCTION

As traditional fossil energy reserves are gradually decreasing and global population continues to rise, biomass has been an important environmentally friendly renewable energy resource used in construction materials, furniture, and the energy field (Tomak *et al.* 2014; Sun *et al.* 2018). The lignocellulosic biomass of bamboo is a potential feedstock for producing chemicals and fuels by thermochemical and biochemical conversion technology due to its sustainability, high abundance, and carbon-neutral character (Saidur *et al.* 2011; Saidi *et al.* 2014; Ma *et al.* 2019a). However, the use of the lignocellulosic biomass of bamboo for the production of fuels by thermochemical conversion technology has several downsides, which include low energy density, high moisture and oxygen contents, and poor grindability (Lu *et al.* 2013; Tran *et al.* 2013; Xu *et al.* 2015). The thermochemical conversion technologies (torrefaction, pyrolysis, combustion, and gasification) have received attention because they can improve biomass quality by enhancing the chemical structure and physical properties.

Torrefaction was considered as a biomass feedstock pretreatment technology at temperatures between 200 °C and 300 °C under inert atmosphere developed for the lignocellulosic biomass (mainly composed of hemicellulose, cellulose, and lignin) to improve its quality for efficient energy conversion and optimize the lignocellulosic structure of biomass (Chen *et al.* 2016b). The thermal decomposition of lignocellulose involves a series of chemical reactions and transforming mechanisms (Turner *et al.* 2010; Rousset *et al.* 2012). Uemura *et al.* (2017) and Ma *et al.* (2019b) reported that the three components (hemicellulose, cellulose, and lignin) of lignocellulose are decomposed to form oxygen-containing products (CO_2, CO, H_2O, acids, and aldehydes) through dehydroxylation, decarbonylation, and decarboxylation reactions during the torrefaction process (Chen *et al.* 2015). Through these mechanisms, the lignocellulosic biomass transforms raw biomass into a material with higher caloric value, low oxygen content, hydrophobicity, and better grindability. However, the properties of torrefaction products are influenced by several factors, such as biomass composition, temperature, duration, heating rate, and atmosphere (Rodrigues and Rousset 2015).

Much work has been done to study how atmosphere influences torrefaction (Li *et al.* 2015b; Strandberg *et al.* 2015; Xu *et al.* 2017). Recently, several types of atmosphere have been studied to evaluate thermal degradation behaviour, and the most commonly reported method is the use of N_2 for oxygen removal in biomass. Li *et al.* (2015b) found that the bamboo torrefied under carbon dioxide atmosphere was subjected to substantial changes in structure and decomposition of carbohydrates, and the carbon content of biomass was enhanced considerably. Ma *et al.* (2019b) and Chen *et al.* (2018b) investigated the influence of the ammonia torrefaction and fast pyrolysis processes on the production of N-containing chemicals. They concluded that the content of nitrogen increased from 0.03% to 7.59% in torrefied bamboo, the concentration of N-containing chemicals in bio-oil dramatically increased, and the highest content of N-containing chemicals was 27.5% in NH_3 atmosphere when the pyrolysis temperature was 850 °C. NH_3 caused the decomposition reactions and generated H radicals, NH_2^* radicals, and NH^* radicals. In addition, NH_3 reacted with –C=O and –OH to inhibit the generation of O-containing compounds, such as ketones, aldehydes, and acids, *etc*.

As a cheap and efficient gas in the atmosphere, oxygen has been widely used for fuel, in the energy field, and by thermochemical conversion technology to reduce operating costs and energy consumption. However, past research has mainly focused on the qualitative analysis of the products at different conditions and did not focus on the torrefaction and pyrolysis product quantitative and semi-quantitative analyses (Rousset *et al.* 2012; Conag *et al.* 2018). Thus, it is important to explore the effect of oxygen concentrations on the characteristics of torrefied products and perform quantitative analysis.

In this study, different oxygen concentrations in the process of bamboo torrefaction pretreatment were investigated to examine the thermal reactivity and quantitative analysis of torrefied bamboo products relative to the mass and energy yield of the torrefaction process. Moreover, the oxygen torrefied biomass was pyrolyzed in Py-GC/MS to produce high value-added chemicals and investigate the formation mechanism of O-containing compounds in bio-oil. These obtained results provided a useful and novel method to upgrade biomass *via* torrefaction and pyrolysis.

EXPERIMENTAL

Materials

Five-year-old moso bamboo (*Phyllostachys edulis*) was collected from a bamboo processing factory in Zhejiang Province (Jiande Muke Ecological Agricukture Co., Ltd., Jiande, China). The moso bamboo was milled into powder using a grinder (Wuyi Haina Instrument Technology Co., Ltd., Beijing, China). Bamboo powder with particle sizes between 75 μm and 150 μm was used for the experiments. The bamboo powder was dried at 80 °C for 6 h to remove water before the torrefaction experiment.

Oxygen Torrefaction Experiment

The torrefaction experiments with different oxygen concentrations were performed in the temperature-controlled tube furnace shown (Bo Yuntong Instrument Technology Co., Ltd., Nanjing, China) in Fig. 1. Approximately 5 g of bamboo powder was placed in a quartz crucible with fixed torrefaction temperatures of 200 °C, 250 °C, and 300 °C and a fixed heating rate of 10 °C ·min^{-1}. The samples were held for 30 min. The mixed gas was used as carrier gas with a fixed flow rate of 200 mL·min^{-1}. The gas mass flow controller was used to control the input of volume flow of nitrogen and oxygen to achieve different oxygen concentrations atmosphere, and the volume flow of nitrogen and oxygen was shown in the control panel, respectively. The torrefied solid product was further cooled in a desiccator for mass and other analysis. The torrefied liquid products were collected in the condenser using a cold trap and -20 °C ethanol, and the gaseous products were collected in a gas collection bag. The bamboo torrefied in nitrogen and 3%, 6%, and 9% oxygen concentration atmospheres at different temperatures were labeled as BTN-200, BTN-250, BTN-300, BTO-300-3, BTO-300-6, and BTO-300-9, respectively. To reduce experimental error, the experiment was repeated three times under the same conditions. The mass and energy yield of the torrefied solid product were calculated using Eqs. 1 and 2:

$$\text{Mass yield (\%)} = \frac{\text{Mass of torrefied bamboo}}{\text{Mass of raw bamboo}} \times 100 \quad (1)$$

$$\text{Energy yield (\%)} = \text{Mass yield} \times \frac{\text{HHV}_{\text{torrefied bamboo}}}{\text{HHV}_{\text{raw bamboo}}} \times 100 \quad (2)$$

After the torrefaction experiments were accomplished, the liquid and gaseous products were collected from the condensate tube and gas collection bag, respectively. The mass yield of solid and liquid products was determined by weighing, and the mass yield of gaseous product was calculated according to Eq. 3:

$$\text{Gaseous yield} = 100\% - \text{Yield of solid (\%)} - \text{Yield of liquid (\%)} \quad (3)$$

Pyrolysis Experiment

The tube furnace (TL1200; Nanjing BYT Instrument Technology Co., Ltd., Nanjing, China) was used for torrefied bamboo pyrolysis, and its schematic diagram is shown in Fig. 1. The temperature-controlled tube furnace were composed of a mass flow controller, thermo-controller, tubular furnace, and condensation system. The mass flow controller was used to control the input of volume flow of nitrogen and oxygen to achieve different oxygen concentrations atmosphere, and the volume flow of nitrogen and oxygen was shown in the control panel, respectively. The thermo-controller was used to control fixed temperature and the temperature program settings. The tubular furnace was mainly

used for torrefaction and pyrolysis experiments, and the condensation system was used for collecting the condensable gas. In each test, approximately 5 g of the raw or torrefied bamboo was placed in a ceramic boat, and then the ceramic boats were placed in the top of a quartz tube. First, the vacuum pump was used to exhaust the air in the quartz tube. Next, the high-purity N_2 or mixed gas (high-purity N_2 and high-purity O_2) was injected into the quartz tube until the pressure reached atmospheric pressure. Finally, the furnace was heated from room temperature to target temperature (850 °C) at a heating rate of 10 °C·min^{-1} and a fixed flow rate (200 mL·min^{-1}), and the ceramic boat was rapidly moved from the top to the center of tube furnace. The terminal temperature was maintained for 30 min. Once the temperature fell to room temperature, the solid product was taken out to calculate the yield and further analyze their physicochemical characteristics.

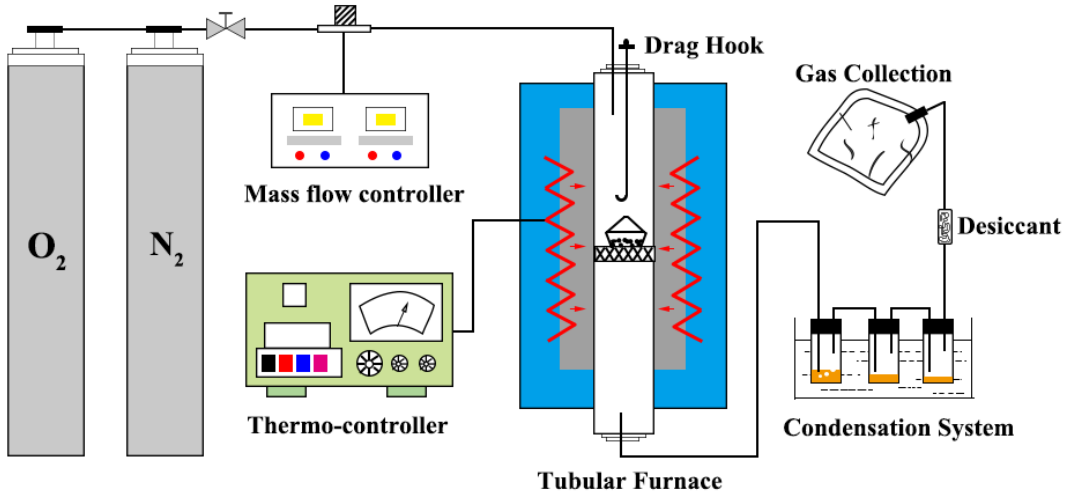

Fig. 1. The temperature-controlled tube furnace setup

Analysis Methods

The ultimate analysis of raw and torrefied bamboo was measured *via* an elemental analyzer (Vario EL III; Elementar Analysensysteme GmbH, Hanau, Germany) according to the CHNS model (Ma *et al.* 2019c). The percentage of oxygen present was determined by the balance. The higher heating value (HHV) was calculated according to Eq. 4 based on the elemental content data (Yin 2011; Dava *et al.* 2017). The symbols C, H, and O in Eq. 4 represent the weight percentages of carbon, hydrogen, and oxygen, respectively, in the solid.

$$HHV\ (MJ/kg) = 32.7934 + 0.0053C^2 - 0.5321C - 2.8769H + 0.0608CH - 0.2401N \quad (4)$$

A Fourier transform infrared spectrometer (Nicolet 6700; Thermo Fisher Scientific, Waltham, MA, USA) was used to characterize the chemical functional groups in moso bamboo during torrefaction. The mass ratio of torrefied bamboo to KBr was 100, and it was ground to pass through a 200-mesh screen. The FTIR spectra were recorded in the wavenumber range 4000 cm^{-1} and 500 cm^{-1} with a resolution of 4 cm^{-1} and a spectrum scan time of 8 s.

PY-GCMS was used for qualitative analysis of the liquid organic compounds from the pyrolysis process of the torrefied bamboo. The organic compounds released from the pyrolysis process were analyzed using a pyrolyzer (CDS 5200; Boside Technology Co., Ltd., Beijing, China) and a gas chromatograph/mass spectrometer (5977B–7890B; Agilent

Technologies, Santa Clara, CA, USA). In each experiment, approximately 0.2 mg of raw or torrefied bamboo was placed into the quartz filler tube, and then the temperature of the pyrolyzer was increased to the target pyrolysis temperature (850 °C) at a heating rate of 20 °C·ms^{-1} and a fixed residence time of 20 s. The injector and transfer line temperature were maintained at 300 °C. The HP-5MS capillary column (30 m × 0.25 mm inner diameter × 0.25 μm film thickness) (Agilent Technologies, Santa Clara, CA, USA) was used for chromatographic separation. The GC oven temperature was increased to 40 °C for 3 min, raised to 290 °C at a heating rate of 10°C·min^{-1}, and maintained for 3 min. The carrier gas was helium (99.999%) with a fixed flow rate of 3 mL·min^{-1}. Furthermore, the mass spectra were obtained in the mass-to-charge ratio range of 50 to 400. Based on the NIST library and the relevant literature, each chromatographic peak was identified using Mass Hunter Workstation Software (Agilent Technologies, Santa Clara, CA, USA). The relative content of each compound was determined by the corresponding peak area. Details of the experimental information were reported by Ma *et al.* (2019a,c).

RESULTS AND DISCUSSION

Product Distribution

Figure 2 shows the product distribution of bamboo during torrefaction under a nitrogen and 9% oxygen atmosphere. The detailed of the mass yield of solid, liquid, and gas were as shown in Table 1. When the torrefaction temperature increased from 200 to 300 °C in nitrogen, the mass yield of solid gradually decreased from 96.6% to 47.2%, whereas the mass yield of liquid product remarkably increased from 1.39% to 20.6%. The mass yield of gas gradually increased from 1.97% to 32.2%.

Table 1. Details of the Mass Yield of Solid, Liquid, and Gas in Nitrogen and Different Oxygen Concentration Atmosphere during Torrefaction

Mass / Sample	Solid (%)	Liquid (%)	Gaseous (%)	Moisture(%)
Raw	100.00	0.00	0.00	7.43±0.16
BTN-200	96.64±0.96	1.39±0.01	1.97±0.01	3.75±0.11
BTO-200-3	96.60±0.93	1.72±0.01	1.68±0.01	3.94±0.13
BTO-200-6	96.56±0.93	2.15±0.02	1.29±0.01	6.32±0.13
BTO-200-9	95.32±0.95	2.30±0.02	2.38±0.02	9.20±0.16
BTN-250	82.10±0.82	11.32±0.09	8.58±0.04	3.64±0.13
BTO-250-3	74.09±0.74	18.51±0.11	7.40±0.03	4.01±0.10
BTO-250-6	68.27±0.68	19.81±0.12	11.92±0.08	4.85±0.11
BTO-250-9	53.75±0.54	23.70±0.14	22.55±0.22	7.74±0.13
BTN-300	47.23±0.47	20.59±0.12	32.18±0.32	2.06±0.08
BTO-300-3	43.50±0.44	20.94±0.13	35.56±0.36	4.90±0.12
BTO-300-6	38.98±0.39	21.79±0.13	17.19±0.17	7.08±0.16
BTO-300-9	31.67±0.32	32.28±0.19	36.05±0.36	7.45±0.16

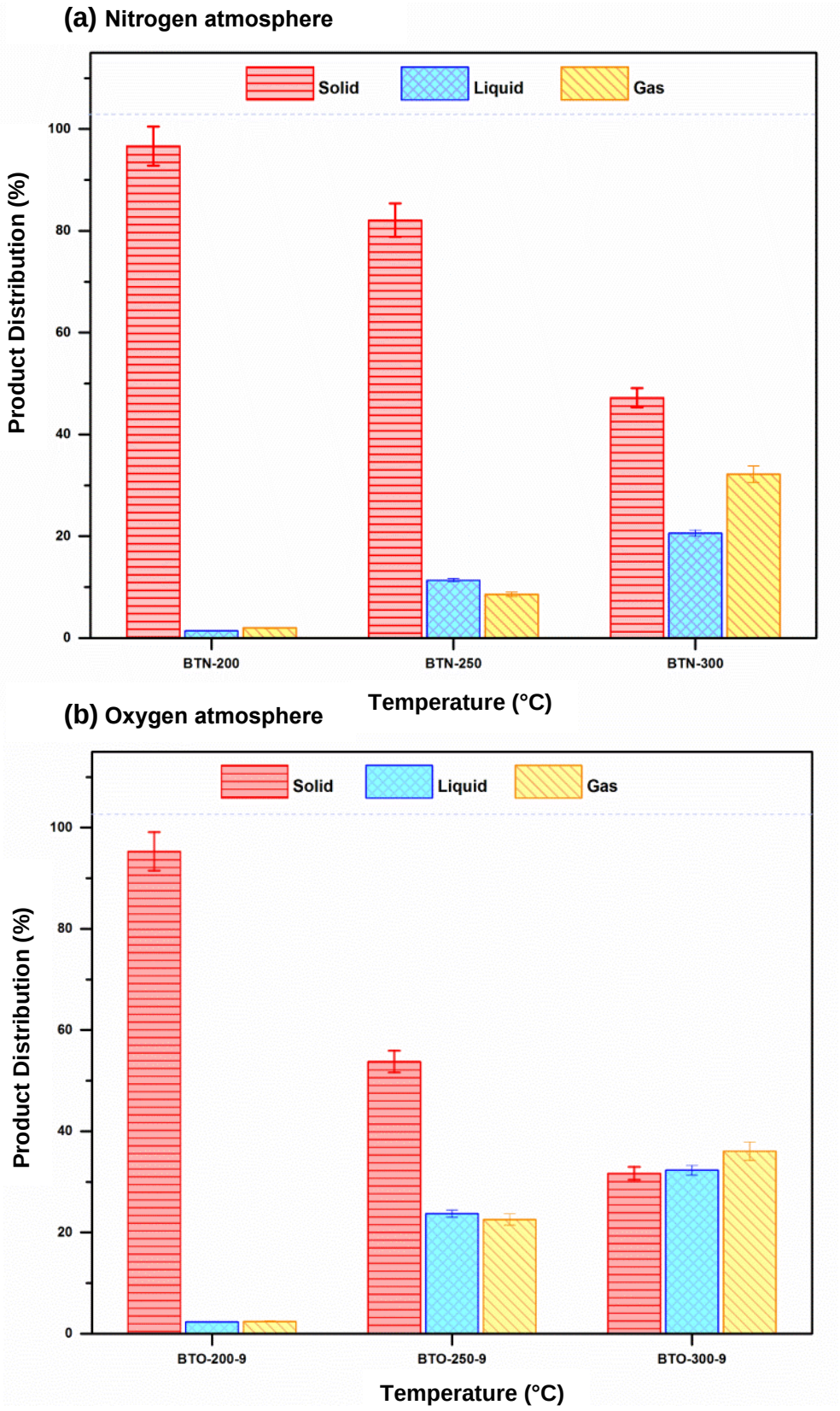

Fig. 2. The mass yield of solid, liquid, and gas products from bamboo torrefaction at different temperature under a nitrogen and 9% oxygen concentration atmosphere

For the oxygen torrefied bamboo, the mass yields of solid, liquid, and gas showed similar trends to those in nitrogen. However, when the torrefaction temperature was increased from 200 °C to 300 °C under a 9% oxygen atmosphere, the mass yield of solid product decreased remarkably at each corresponding torrefaction temperature, and the mass yield of solids decreased from 95.3% to 31.7%. The mass yields of liquid and gas increased substantially, and the final yields at 300 °C were 32.3% and 36.0%, respectively. In the different oxygen concentration ranges of 3% to 9%, the solid yield gradually decreased as oxygen concentration increased, and the mass yields of liquid and gas showed opposite tendencies. This was mainly because many volatiles were previously released during the torrefaction process, and thermal cracking and oxidative reactions occurred under oxygen atmosphere (Bach *et al.* 2017; Chen *et al.* 2018a).

Ultimate Analysis, Mass, and Energy Yield

The data of the elemental, mass yield, energy yield, and calorific analysis of the raw and torrefied bamboo are shown in Table 2.

Table 2. Effect of Torrefaction Temperature and Oxygen Concentrations on Elemental Analysis, Mass Yield, and HHV of Raw and Torrefied Bamboo

Properties	Mass Yield (%)	C (wt%)	H (wt%)	O (wt%)	N (wt%)	S (wt%)	HHV (MJ/kg)	Ash (wt%)	EY (%)
Raw	100± 0.00	47.53 ± 0.14	6.35± 0.19	42.95 ± 0.13	3.16 ± 0.09	0.01± 0.01	18.80± 0.52	3.26 ±0.08	100± 0.00
BTN-200	96.64 ±0.77	48.83 ± 0.16	6.28± 0.17	41.57 ± 0.10	3.29 ± 0.06	0.03± 0.01	19.24± 0.48	4.12 ±0.07	99.90± 0.28
BTO-200-3	96.60 ±0.70	48.59 ± 0.15	6.26± 0.17	41.50 ± 0.12	3.63 ± 0.08	0.02± 0.01	19.06± 0.51	4.35 ±0.10	99.31± 0.27
BTO-200-6	96.56 ±0.68	48.87 ± 0.15	6.25± 0.14	41.02 ± 0.15	3.84 ± 0.07	0.02± 0.02	19.12 ±0.59	6.32 ±0.11	99.92± 0.26
BTO-200-9	95.32 ±0.70	48.96 ± 0.16	6.15± 0.16	40.89 ± 0.12	3.95 ± 0.07	0.05± 0.02	19.11 ±0.53	8.25 ±0.13	98.43± 0.29
BTN-250	82.10 ±0.56	53.58 ± 0.18	6.07± 0.14	35.98 ± 0.16	4.34 ± 0.06	0.03± 0.01	20.77 ±0.76	10.10 ±0.12	95.68± 0.16
BTO-250-3	74.09 ±0.57	54.57 ± 0.16	5.81± 0.14	34.82 ± 0.13	4.76 ± 0.07	0.04± 0.02	20.96 ±0.77	12.90 ±0.12	87.07± 0.17
BTO-250-6	68.27 ±0.60	57.11 ± 0.16	5.57± 0.12	32.60 ± 0.15	4.66 ± 0.06	0.06± 0.01	21.89 ±0.68	13.04 ±0.13	83.82± 0.14
BTO-250-9	53.75 ±0.77	67.28 ± 0.20	3.22± 0.13	24.22 ± 0.19	5.23 ± 0.08	0.05± 0.02	23.64 ±0.66	14.13 ±0.14	70.86± 0.16
BTN-300	47.23 ±0.68	69.34 ± 0.33	5.17± 0.16	20.41 ± 0.16	5.05 ± 0.09	0.03± 0.01	27.09 ±0.78	13.04 ±0.11	73.48± 0.15

BTO-300-3	43.50 ±0.67	66.74 ± 0.31	4.55± 0.13	23.67 ± 0.15	4.99 ± 0.10	0.05± 0.01	25.06 ±0.74	13.33 ±0.12	61.85± 0.16
BTO-300-6	38.98 ±0.71	68.13 ± 0.32	3.57± 0.11	22.69 ± 0.16	5.55 ± 0.07	0.06± 0.02	24.33 ±0.75	14.29 ±0.14	53.75± 0.13
BTO-300-9	31.67 ±0.66	68.88 ± 0.36	2.89± 0.13	22.27 ± 0.14	5.89 ± 0.07	0.07± 0.03	23.66 ±0.76	14.43 ±0.16	42.51± 0.16

As the torrefaction temperature increased from 200 °C to 300 °C, the mass yield gradually decreased from 96.6% and 96.6% to 47.2% and 31.7% in nitrogen and oxygen, respectively. The result showed that oxygen effectively influenced the solid mass yield. The energy yield of torrefied solid product gradually decreased from 98.9% to 30.8%. The mass yield and energy yield decreased as temperature and oxygen concentration increased, and previous reports observed a similar trend (Uemura *et al.* 2013; Chen *et al.* 2014). The HHV of the original bamboo was 18.8 MJ/kg, and it increased to 27.1 MJ/kg and 23.7 MJ/kg when bamboo was torrefied at 300 °C under nitrogen and 9% oxygen, respectively. However, the HHV of the torrefied bamboo was lower than that of torrefied bamboo at 250 °C under an oxygen atmosphere. This result indicated that a small amount of oxygen mainly provided extra energy by reducing the low-energy bonds and increasing the high-energy bonds (C−C) (Liu *et al.* 2013; Li *et al.* 2015).

Figure 3 shows elemental analysis results for the raw and torrefied bamboo. The carbon content increased from 47.5% to 68.9%, and the oxygen content decreased from 43.0% to 22.3%. In particular, the hydrogen content decreased dramatically from 6.35% to 2.89%. This result was attributed to the oxidative reaction in the torrefaction process under an oxygen atmosphere (Li *et al.* 2015a). Ma *et al.* (2019c) reported that oxygen was mainly released in the forms of H_2O, CO_2, and CO by dehydroxylation, decarbonylation, and decarboxylation reactions during the torrefaction process. The carbon, oxygen and hydrogen concentrations of the raw bamboo were 47.5%, 43.0%, and 6.35%, respectively. When the torrefaction temperature was at 200 °C and 250 °C and the oxygen concentrations increased from 3% to 9%, the carbon sharply increased from 48.8% to 67.9%, and the oxygen and hydrogen decreased from 41.6% and 6.28% to 24.2% and 3.22%, respectively. However, the contents of carbon and hydrogen gradually decreased from 69.3% and 5.17% to 68.9% and 2.89%, respectively, as the oxygen concentrations increased. However, oxygen content had the opposite trend, as it increased from 20.4% to 22.3% at 300 °C. Based on the results of the elemental contents, the oxygen concentrations affected the elemental distribution (Bilbao *et al.* 1997). Specifically, a lower oxygen concentration torrefaction pretreatment could effectively remove oxygen and improve the use potential of bamboo in the energy field.

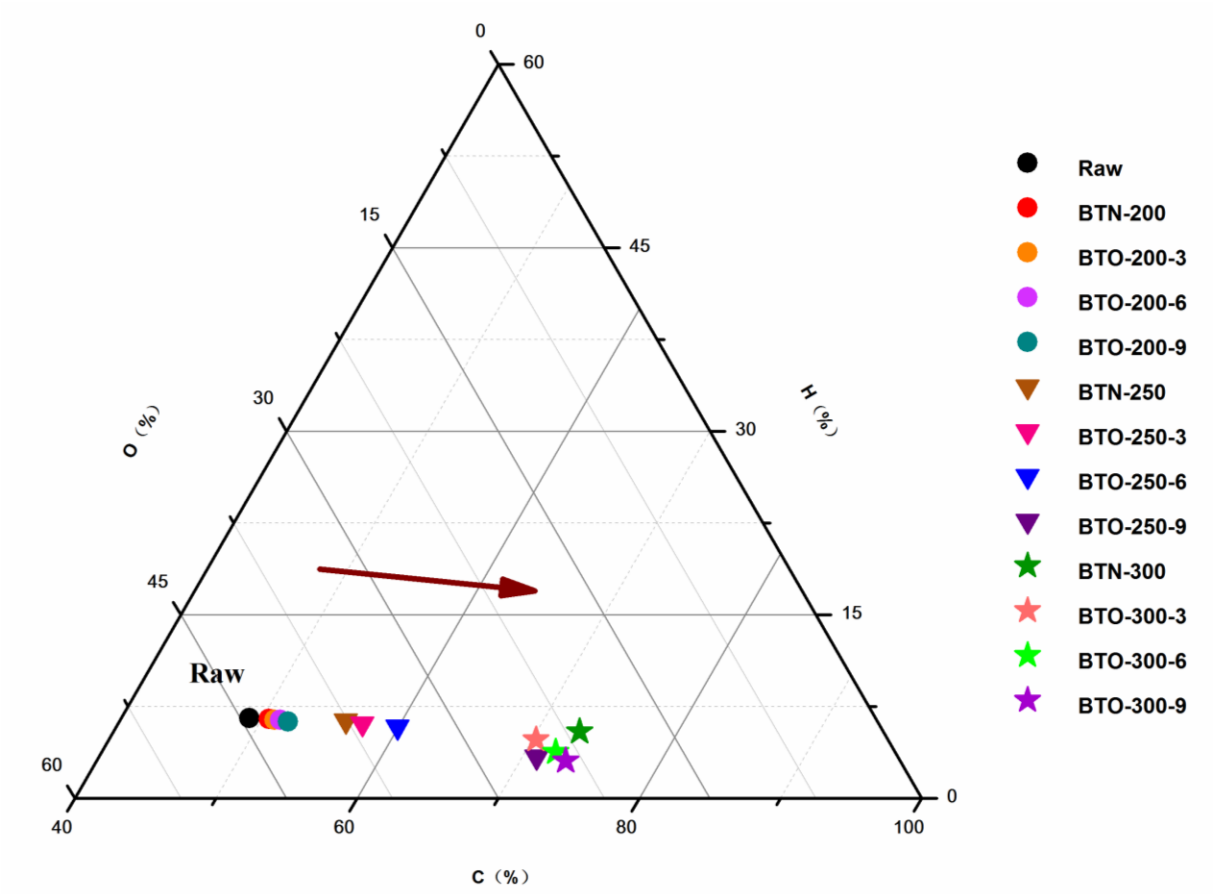

Fig. 3. Diagram of C, H, and O analysis at different torrefaction temperatures and atmospheres

FTIR Analysis

Figure 4 shows the effect of torrefaction temperatures and oxygen concentrations on the chemical functional groups of the bamboo. Five remarkable characteristic infrared absorbance bands with absorbance at 3460 cm^{-1}, 2819 cm^{-1}, 1706 cm^{-1}, 1680 cm^{-1} to 1440 cm^{-1}, and 1190 cm^{-1} to 950 cm^{-1} were observed. The band at 3460 cm^{-1} was attributed to the stretching vibration of the O−H band in the H_2O, which was mainly related to cracking from the hydroxyl linked on the phenolic and aliphatic structure or the combustion reaction between hydrogen and oxygen elements during the oxygen torrefaction process (Ma *et al.* 2018a, 2018b). The band at 2819 cm^{-1} was ascribed to the stretching vibration of C−H, which was derived from the methoxy groups, methyl, and the methylene in aliphatic or alkanes (Chen *et al.* 2016a). The band at 1706 cm^{-1} was attributed to the C = O stretching vibration in the aldehydes, ketones, and organic acids that contained the carboxyl and carbonyl functional groups (Zhen-Yu *et al.* 2017). The absorbance peak in the range 1680 to 1440 cm^{-1} was caused by the stretching vibration of C = C from the benzene ring in aromatics (Esteves *et al.* 2013). The band between 1190 cm^{-1} to 950 cm^{-1} was the fingerprint region, which was derived from C−O and C−H linked on the syringyl, guaiacyl, and hydroxyphenyl. Therefore, the characteristic absorbance bands between 1190 cm^{-1} and 950 cm^{-1} may have represented alcohols, esters, and ethers compounds (Ma *et al.* 2015; Lin *et al.* 2018).

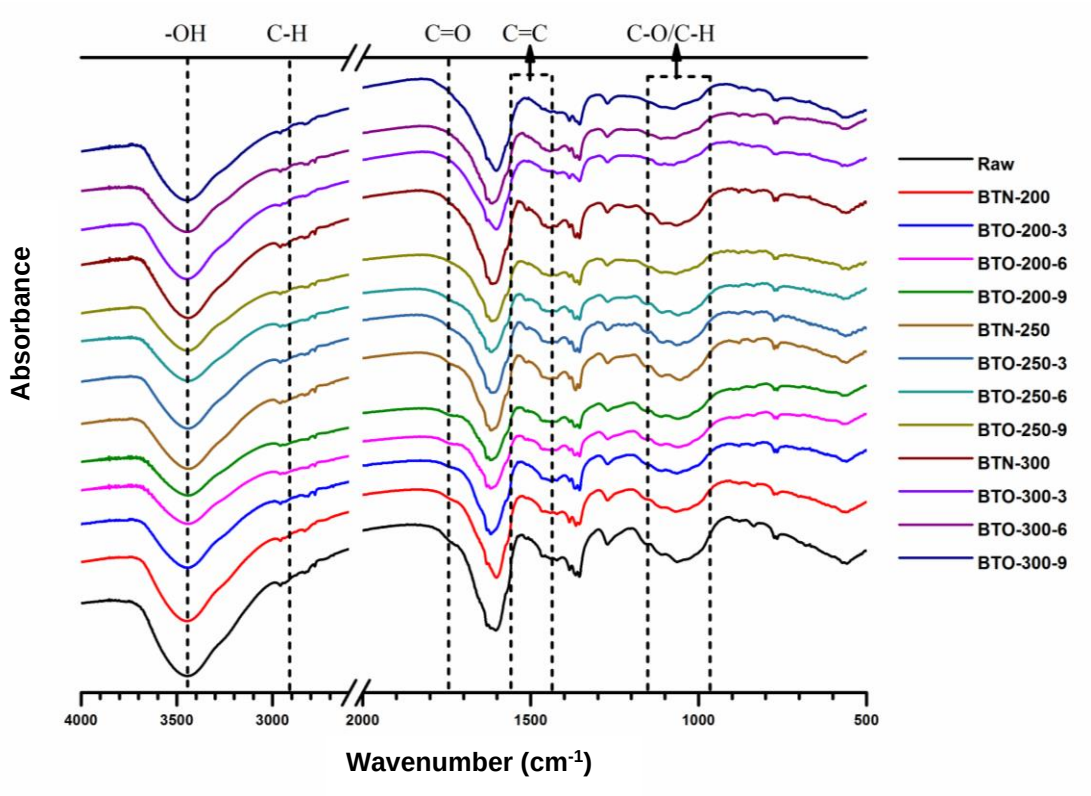

Fig. 4. The FTIR analysis of the raw and torrefied bamboo

The absorbance intensity of the above five characteristic adsorption bands decreased as the torrefaction temperature was increased from 200 °C to 300 °C. Wang *et al.* (2009) reported that the intensity of absorbance was linearly dependent on the relative content of the functional groups. As the temperature increased, the intensity of O−H decreased, which was attributed to the occurrence of deacetylation reactions during the torrefaction process, which resulted in the formation of H_2O to enhance the bamboo hydrophobicity (Xu *et al.* 2019). The absorbance of C−H at 2819 cm^{-1} decreased remarkably, which indicated the breakage of methyl and methylene linked to the basic units in hemicellulose and cellulose. The band of methyl and methylene exhibited a reduced intensity, which was due to hemicellulose and cellulose thermal cracking (Liang and Xue 2013). The decreased intensity of C = O was attributed to the presence of decarboxylation and decarbonylation reactions (Popescu *et al.* 2013). The C=C corresponding absorbance peak stretching vibration or the benzene ring skeleton became slightly weaker when the torrefaction temperature was increased from 200 °C to 300 °C. Due to the methyl and methoxy cracking under the hemicellulose, cellulose and lignin thermal degradation of the C-H/C-O stretching vibration intensity clearly decreased (Chih *et al.* 2019).

Further, the oxygen concentrations had an obvious effect on the types and content of functional groups on the surface of biomass. The presence of oxygen resulted in the gradual decrease of the intensity of five characteristic infrared absorbance bands. This result indicated that the extra energy was provided to accelerate deoxygenation reactions, such as dehydration, decarbonylation, and decarboxylation reactions, in the lower oxygen concentration at each corresponding torrefaction temperature. However, when oxygen concentration increased from 6% to 9%, the absorbance intensity of the five characteristic bands decreased slightly, which was also reported Dai *et al.* (2017). Liang and Xue (2013)

and Bilbao *et al.* (1997) reported the effect of oxygen percentage on the contents of biomass surface functional groups. Therefore, as torrefaction temperature and oxygen concentrations increased, the intensity of a series of characteristic absorbance peaks gradually decreased.

Py-GC/MS Analysis

For qualitative analysis, Py-GC/MS was used on the organic compounds of bio-oil from fast pyrolysis of raw and torrefied bamboo, and the details of each component and relative contents are shown in Tables S1 through S4 in the Appendix (supplementary material). Figure 5 shows the effect of torrefaction temperatures (200 °C, 250 °C, and 300 °C) and oxygen concentration (3%, 6%, and 9%) on the relative contents of components in the pyrolysis (850 °C) liquid product. The total area of each component of bio-oil was less than 100% because several components were present in minimal amounts that were not counted. According to the characteristic functional groups, the bio-oil components were mainly classified into eight groups, which were acids, furans, phenols, ketones, aldehydes, esters, alcohols, and hydrocarbons.

Figure 5a in supplementary file shows the effect of torrefaction temperature on the relative contents of components in the pyrolysis liquid product. As the torrefaction temperature gradually increased, the relative content of acids, furans, ketones, and alcohols decreased from 13.6%, 16.6%, 9.48%, and 9.48% to 9.66%, 13.1%, 3.91%, and 7.16%, respectively. The decreases in furans, ketones, and alcohols were attributed to ring-opening and depolymerization reactions in cellulose and hemicellulose during the torrefaction process (Werner *et al.* 2014). The formation of small molecular acids was mainly due to the thermal properties of hemicellulose, which formed the breakage of O-acetyl groups linked on the xylan side chains at the C_2 position and the ring-opening reaction of the 4-O-methylglucuronic acid unit. Further, the long-chain fatty acids decreased notably at higher torrefaction temperatures (Shen *et al.* 2010). The content of phenols and hydrocarbons increased from 35.9% to 6.55% to 43.9% and 12.7%, respectively. The dominant phenols were directly obtained from cleavage of β−O−4 linkages in lignin. The higher torrefaction temperatures promoted the above pyrolysis reaction, which resulted in the increase in the relative content of phenols (Ma *et al.* 2019c). The hydrocarbons were mainly derived from the dehydrated product of hemicellulose cellulose−dehydrated sugars, which resulted from a series of dehydration, decarboxylation, decarbonylation, and oligomerization reactions (Zheng *et al.* 2014).

Figure 5b through 5d in supplementary file shows that compared with nitrogen atmosphere, the oxygen concentrations had a noticeable influence on the relative content of organic compounds present in the bio-oil. As the oxygen concentration increased from 3% to 9%, the relative content of acids initially decreased from 13.4% to 7.92% and then increased to 15.3% at torrefaction temperatures of 200 °C to 300 °C. Acetic acid was the dominant component in bio-oil, and the relative content of acetic acid disappeared when oxygen concentrations increased.

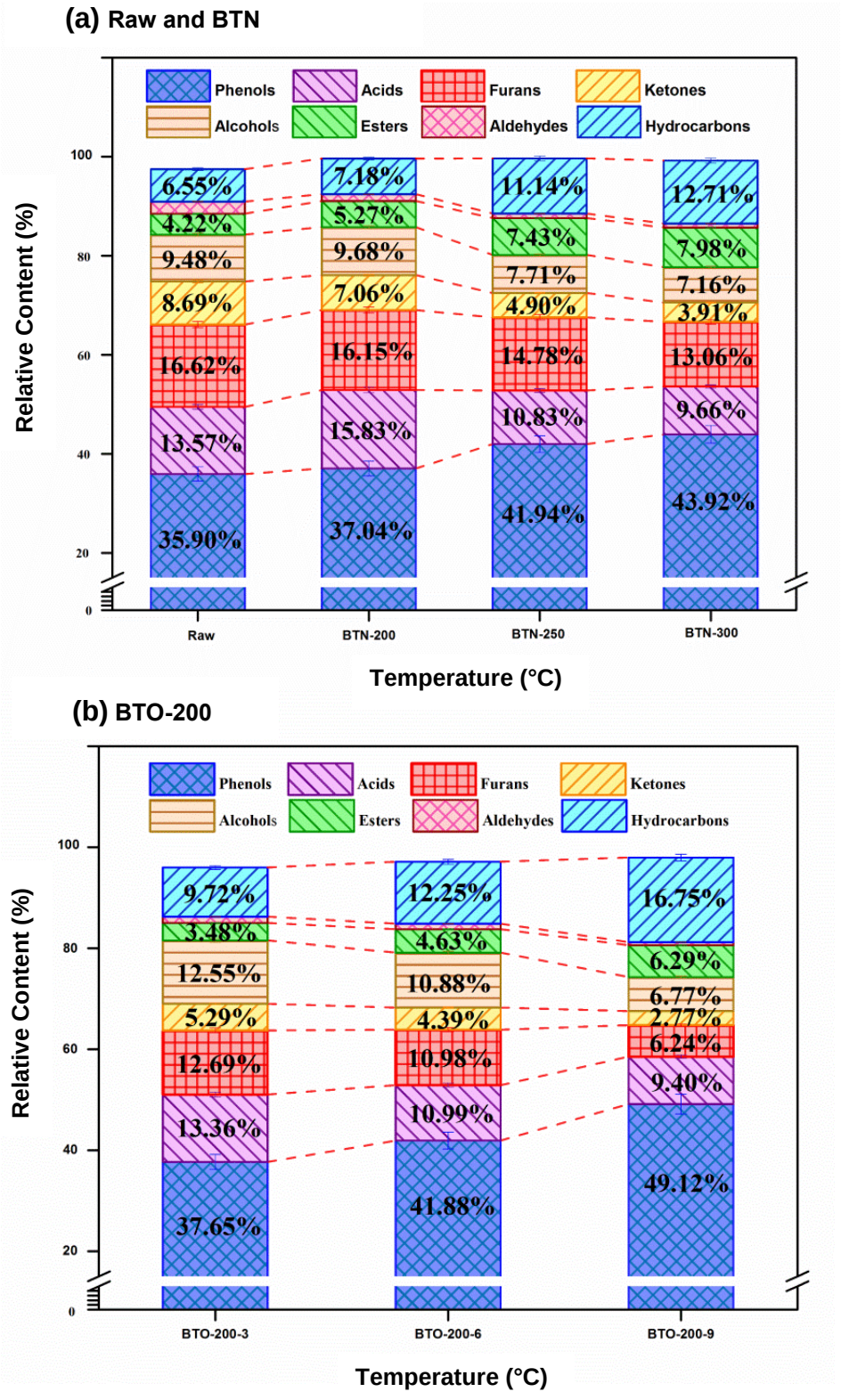
(a) Raw and BTN
Phenols
Acids
Furans
Ketones
Alcohols
Esters
Aldehydes
Hydrocarbons
Relative Content (%)
6.55%
4.22%
9.48%
8.69%
16.62%
13.57%
35.90%
7.18%
5.27%
9.68%
7.06%
16.15%
15.83%
37.04%
11.14%
7.43%
7.71%
4.90%
14.78%
10.83%
41.94%
12.71%
7.98%
7.16%
3.91%
13.06%
9.66%
43.92%
Raw
BTN-200
BTN-250
BTN-300
Temperature (°C)
(b) BTO-200
Phenols
Acids
Furans
Ketones
Alcohols
Esters
Aldehydes
Hydrocarbons
Relative Content (%)
9.72%
3.48%
12.55%
5.29%
12.69%
13.36%
37.65%
12.25%
4.63%
10.88%
4.39%
10.98%
10.99%
41.88%
16.75%
6.29%
6.77%
2.77%
6.24%
9.40%
49.12%
BTO-200-3
BTO-200-6
BTO-200-9
Temperature (°C)

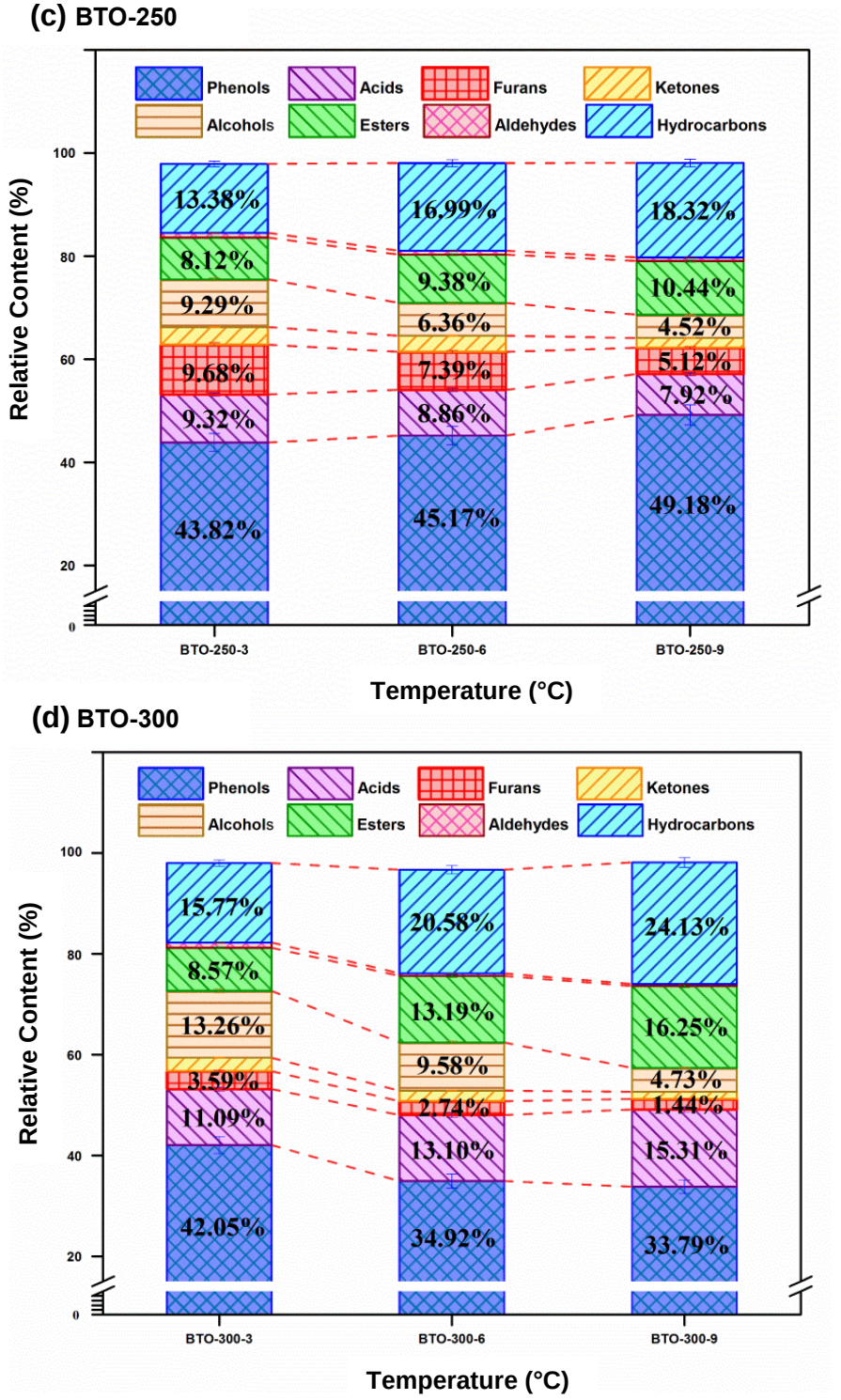

Fig. 5. Effect of torrefaction temperatures and oxygen concentrations on the relative contents of pyrolysis liquid components

The mechanism of the formation of acetic acid was involved with the elimination reaction of the O-acetyl groups linked to the xylan chain on C_2 position and another path of the formation of acetic acid was the elimination reaction of the ketene structure of the fragment from the 4-O-methylglucuronic acid unit. Therefore, the O-acetyl groups and 4-O-methylglucuronic acid unit not only exhibited a thermal degradation reaction, but this

also was accompanied by a combustion reaction at lower oxygen concentration, resulting in decreased relative content of acids (Shen *et al.* 2010, 2015). Branca and Di Blasi (2004) also found the biomass decomposition in oxidative was a two-stage process, the first of which was devolatilization. The second stage was char combustion reactions, which resulted in the content of acids sharply decreasing.

The relative content of furans, ketones, and aldehydes decreased from 12.7%, 5.29%, and 1.24% to 2.09%, 1.44%, and 0.39%, respectively. The decrease in furans was mainly attributed to the ring-opening and depolymerization reactions of the basic structural units in hemicellulose and cellulose (Werner *et al.* 2014). The formation of ketones from the cracking of xylan-chain units might be accelerated by oxygen, which would result in the decrease of evolution of ketones. Further, the xylan-chain cracking could have been oxidative decomposition of smaller molecules, such as water, CO, and CO_2 (Shen *et al.* 2013). The evolution of aldehydes remarkably decreased as the oxygen concentration was increased, which was due to the presence of oxygen promoting the break of C−C bonds, eliminating the fragments with the ending groups of −CHO or –CHOH, and the oxidation of hydroxyl groups in raw material under the same conditions (Shen *et al.* 2015). Therefore, higher torrefaction and oxygen concentrations enhanced the decomposition of O-containing compounds.

As oxygen concentration increased, the relative content of esters increased from 3.48% to 16.2%. However, the relative content of alcohols showed the opposite tendency, as it decreased from 12.6% to 4.73%. This result indicated that the relative content of alcohols was inhibited and gradually decreased by the increasing oxygen concentrations, which were ascribed to the enhancement of oxidative decomposition. The formation of esters was mainly produced by the neutralization reaction at higher temperatures (Xu *et al.* 2019).

Phenols were produced by the thermal degradation of lignin. The oxygen concentration increased from 3% to 6%, and the relative content of phenols increased from 37.6% to 49.2% when the torrefaction temperature was increased from 200 °C to 250 °C. This was attributed to the breakage of C-C bonds in the lignin phenylpropane side chain and benzene ring and β−O−4 and α–O–4 linkages in the lignin. However, when oxygen concentrations increased from 6% to 9% at 300 °C, the relative content of phenols decreased from 49.2% to 33.8%. This result indicated that torrefaction pretreatment led to lignin enrichment to form char and then inhibited the formation of phenols at higher torrefaction temperatures (Xue *et al.* 2016). The relative content of hydrocarbons increased from 9.72% to 24.1%. The increase in hydrocarbons was mainly ascribed to the thermal decomposition of hemicellulose and cellulose. However, at a fixed torrefaction temperature of 300 °C, the 3,5-dimethoxy-4-hydroxytoluene and naphthalene were the dominant components in hydrocarbons and tended to form char by the polymerization and polycondensation reactions at higher pyrolysis temperatures (Tao *et al.* 2015). Therefore, lower torrefaction temperatures and oxygen concentrations were preferred for the production of phenols and small molecule hydrocarbon substances.

CONCLUSIONS

1. In this work, the torrefaction temperatures and oxygen concentrations remarkably influenced the pyrolysis of bamboo. The torrefaction liquid product was increased from 1.39% to 32.3% as the oxygen concentrations increased from 3% to 9%.

2. Based on the Py-GC/MS analysis, the phenols and hydrocarbons were the dominant components in bio-oil, and they had relative contents of 33.8% to 49.2% and 6.55% to 24.1%, which attributed to the thermal decomposition of hemicellulose and cellulose basic units.
3. The maximum relative content of phenols was 49.2%, which was obtained at a torrefaction temperature of 250 °C and a pyrolysis temperature of 850 °C. Lower torrefaction temperatures (250 °C) and moderate oxygen concentrations (6%) were optimal for the production of phenols and hydrocarbons. Therefore, the oxygen torrefaction pretreatment was an innovative method, and it can be used for upgrading biomass and its pyrolytic liquid products.

ACKNOWLEDEMENTS

This research was supported by the Major Project of Zhejiang (2018C02008) and the Young Elite Scientists Sponsorship Program by CAST (2018QNRC001). Yi Sun, Zhongqing Ma, and Wenbiao Zhang contributed equally to this work.

REFERENCES CITED

Bach, Q. V., Trinh, T. N., Tran, K.-Q., and Thi, N. B. D. (2017). "Pyrolysis characteristics and kinetics of biomass torrefied in various atmospheres," *Energy Conversion and Management* 141, 72-78. DOI: 10.1016/j.enconman.2016.04.097

Bilbao, R., Mastral, J. F., Aldea, M. E., and Ceamanos, J. (1997). "The influence of the percentage of oxygen in the atmosphere on the thermal decomposition of lignocellulosic materials," *Journal of Analytical and Applied Pyrolysis* 42(2), 189-202. DOI: 10.1016/S0165-2370(97)00050-8

Branca, C., and Di Blasi, C. (2004). "Global interinsic kinetics of wood oxidation," *Fuel* 83(1), 81-87. DOI: 10.1016/S0016-2361(03)00220-5

Chen, D. Y., Gao, A. J., Ma, Z. Q., Fei, D. Y., Chang, Y., and Shen, C. (2018a). "In-depth study of rice husk torrefaction: Characterization of solid, liquid and gaseous products, oxygen migration and energy yield," *Bioresource Technology* 253, 148-153. DOI: 10.1016/j.biortech.2018.01.009

Chen, D. Y., Zhou, J. B., and Zhang, Q. S. (2014). "Effects of torrefaction on the pyrolysis behavior and bio-oil properties of rice husk by using TG-FTIR and Py-GC/MS," *Energy & Fuels* 28(9), 5857-5863. DOI: 10.1021/ef501189p

Chen, T. J., Liu, R. H., and Scott, N. R. (2016a). "Characterization of energy carriers obtained from the pyrolysis of white ash, switchgrass and corn stover—Biochar, syngas and bio-oil," *Fuel Processing Technology* 142, 124-134. DOI: 10.1016/j.fuproc.2015.09.034

Chen, W., Chen, Y. Q., Yang, H. P., Li, K., Chen, X., and Chen, H. P. (2018b). "Investigation on biomass nitrogen-enriched pyrolysis: Influence of temperature," *Bioresource Technology* 249, 247-253. DOI: 10.1016/j.biortech.2017.10.022

Chen, W.-H., Liu, S.-H., Juang, T.-T., Tsai, C.-M., and Zhuang, Y.-Q. (2015). "Characterization of solid and liquid products from bamboo torrefaction," *Applied Energy* 160, 829-835. DOI: 10.1016/j.apenergy.2015.03.022

Chen, W.-H., Zhuang, Y. Q., Liu, S.-H., Juang, T.-T., and Tsai, C. M. (2016b). "Product characteristics from the torrefaction of oil palm fiber pellets in inert and oxidative atmospheres," *Bioresource Technology* 199, 367-374. DOI: 10.1016/j.biortech.2015.08.066

Chih, Y.-K., Chen, W.-H., Ong, H. C., and Show, P. L. (2019). "Product characteristics of torrefied wood sawdust in normal and vacuum environments," *Energies* 12(20), Article ID 3844. DOI: 10.3390/en12203844

Conag, A. T., Villahermosa, J. E. R., Cabatingan, L. K., and Go, A. W. (2018). "Energy densification of sugarcane leaves through torrefaction under minimized oxidative atmosphere," *Energy for Sustainable Development* 42, 160-169. DOI: 10.1016/j.esd.2017.11.004

Dai, G. X., Zou, Q., Wang, S. R., Zhao, Y., Zhu, L. J., and Huang, Q. X. (2017). "Effect of torrefaction on the structure and pyrolysis behavior of lignin," *Energy & Fuels* 32(4), 4160-4166. DOI: 10.1021/acs.energyfuels.7b03038

Daya, N., Muhammad, A. (2017) "HHV predicting correlations for torrefied biomass using proximate and ultimate analyses," *Bioengineering* 4(1), 7. DOI: 10.3390/bioengineering4010007

Esteves, B., Velez Marques, A., Domingos, I., and Pereira, H. (2013). "Chemical changes of heat treated pine and eucalypt wood monitored by FTIR," *Maderas. Ciencia y Tecnología* 15(2), 245-258. DOI: 10.4067/S0718-221X2013005000020

Li, M.-F., Li, X., Bian, J., Chen, C.-Z., Yu, Y.-T., and Sun, R.-C. (2015a). "Effect of temperature and holding time on bamboo torrefaction," *Biomass and Bioenergy* 83, 366-372. DOI: 10.1016/j.biombioe.2015.10.016

Li, M. F., Li, X., Bian, J., Xu, J. K., Yang, S., and Sun, R. C. (2015b). "Influence of temperature on bamboo torrefaction under carbon dioxide atmosphere," *Industrial Crops and Products* 76, 149-157. DOI: 10.1016/j.indcrop.2015.04.060

Liang, Y. F., and Xue, Z. H. (2013). "Effect on the thermal value and inner instructure of biomass under different torrefaction condition," *Advanced Materials Research* 807-809, 795-799. DOI: 10.4028/www.scientific.net/AMR.807-809.795

Lin, B.-J., Colin, B., Chen, W.-H., Pétrissans, A., Rousset, P., and Pétrissans, M. (2018). "Thermal degradation and compositional changes of wood treated in a semi-industrial scale reactor in vacuum," *Journal of Analytical and Applied Pyrolysis* 130, 8-18. DOI: 10.1016/j.jaap.2018.02.005

Liu, Z., Quek, A., Hoekman, S. K., and Balasubramanian, R. (2013). "Production of solid biochar fuel from waste biomass by hydrothermal carbonization," *Fuel* 103, 943-949. DOI: 10.1016/j.fuel.2012.07.069

Lu, K.-M., Lee, W.-J., Chen, W.-H., and Lin, T.-C. (2013). "Thermogravimetric analysis and kinetics of co-pyrolysis of raw/torrefied wood and coal blends," *Applied Energy* 105, 57-65. DOI: 10.1016/j.apenergy.2012.12.050

Ma, Z., Chen, D., Gu, J., Bao, B., and Zhang, Q. (2015). "Determination of pyrolysis characteristics and kinetics of palm kernel shell using TGA–FTIR and model-free integral methods," *Energy Conversion and Management* 89, 251-259. DOI: 10.1016/j.enconman.2014.09.074

Ma, Z. Q., Wang, J. H., Li, C., Yang, Y. Y., Liu, X. H., Zhao, C., and Chen, D. Y. (2019a). "New sight on the lignin torrefaction pretreatment: Relevance between the evolution of chemical structure and the properties of torrefied gaseous, liquid, and solid products," *Bioresource Technology* 288, 121528. DOI: 10.1016/j.biortech.2019.121528

Ma, Z., Wang, J., Yang, Y., Zhang, Y., Zhao, C., Yu, Y., and Wang, S. (2018a). "Comparison of the thermal degradation behaviors and kinetics of palm oil waste under nitrogen and air atmosphere in TGA-FTIR with a complementary use of model-free and model-fitting approaches," *Journal of Analytical and Applied Pyrolysis* 134, 12-24. DOI: 10.1016/j.jaap.2018.04.002

Ma, Z., Wang, J., Zhou, H., Zhang, Y., Yang, Y., Liu, X. H., Ye, J. W., Chen, D., and Wang, S. (2018b). "Relationship of thermal degradation behavior and chemical structure of lignin isolated from palm kernel shell under different process severities," *Fuel Processing Technology* 181, 142-156. DOI: 10.1016/j.fuproc.2018.09.020

Ma, Z., Zhang, Y., Li, C., Yang, Y., Zhang, W., Zhao, C., and Wang, S. (2019b). "N-doping of biomass by ammonia (NH_3) torrefaction pretreatment for the production of renewable N-containing chemicals by fast pyrolysis," *Bioresource Technology* 292, Article ID 122034. DOI: 10.1016/j.biortech.2019.122034

Ma, Z., Zhang, Y., Shen, Y., Wang, J., Yang, Y. Y., Zhang, W., and Wang, S. R. (2019c). "Oxygen migration characteristics during bamboo torrefaction process based on the properties of torrefied solid, gaseous, and liquid products," *Biomass and Bioenergy* 128, Article ID 105300. DOI: 10.1016/j.biombioe.2019.105300

Popescu, M.-C., Froidevaux, J., Navi, P., and Popescu, C.-M. (2013). "Structural modifications of *Tilia cordata* wood during heat treatment investigated by FT-IR and 2D IR correlation spectroscopy," *Journal of Molecular Structure* 1033, 176-186. DOI: 10.1016/j.molstruc.2012.08.035

Rodrigues, T. O., and Rousset, P. L. A. (2015). "Effects of torrefaction on energy properties of *Eucalyptus grandis* wood," *Cerne* 15(4), 446-452.

Rousset, P., Macedo, L., Commandré, J.-M., and Moreira, A. (2012). "Biomass torrefaction under different oxygen concentrations and its effect on the composition of the solid by-product," *Journal of Analytical and Applied Pyrolysis* 96, 86-91. DOI: 10.1016/j.jaap.2012.03.009

Saidi, M., Samimi, F., Karimipourfard, D., Nimmanwudipong, T., Gates, B. C., and Rahimpour, M. R. (2014). "Upgrading of lignin-derived bio-oils by catalytic hydrodeoxygenation," *Energy & Environmental Science* 7(1), 103-129. DOI: 10.1039/C3EE43081B

Saidur, R., Abdelaziz, E., Demirbas, A., Hossain, M., and Mekhilef, S. (2011). "A review on biomass as a fuel for boilers," *Renewable and Sustainable Energy Reviews* 15(5), 2262-2289. DOI: 10.1016/j.rser.2011.02.015

Shen, D. K., Gu, S., and Bridgwater, A. V. (2010). "Study on the pyrolytic behaviour of xylan-based hemicellulose using TG–FTIR and Py–GC–FTIR," *Journal of Analytical and Applied Pyrolysis* 87(2), 199-206. DOI: 10.1016/j.jaap.2009.12.001

Shen, D. K., Ye, J., Xiao, R., and Zhang, H. (2013). "TG-MS analysis for thermal decomposition of cellulose under different atmospheres," *Carbohydrate Polymers* 98(1), 514-521. DOI: 10.1016/j.carbpol.2013.06.031

Shen, D. K., Zhang, L. Q., Xue, J. T., Guan, S. P., Liu, Q., and Xiao, R. (2015). "Thermal degradation of xylan-based hemicellulose under oxidative atmosphere," *Carbohydrate Polymers* 127, 363-371. DOI: 10.1016/j.carbpol.2015.03.067

Strandberg, M., Olofsson, I., Pommer, L., Wiklund-Lindström, S., Åberg, K., and Nordin, A. (2015). "Effects of temperature and residence time on continuous torrefaction of spruce wood," *Fuel Processing Technology* 134, 387-398. DOI: 10.1016/j.fuproc.2015.02.021

Sun, Z., Fridrich, B. L., De Santi, A., Elangovan, S., and Barta, K. (2018). "Bright side of lignin depolymerization: Toward new platform chemicals," *Chemical Reviews* 118(2), 614-678. DOI: 10.1021/acs.chemrev.7b00588

Tao, J., Dong, C. Q., Lu, Q., Liao, H. T., Du, X. Z., Yang, Y. P., and Dahlquist, E. (2015). "Catalytic cracking of biomass high-temperature pyrolysis tar using NiO/AC catalysts," *International Journal of Green Energy* 12(8), 773-779. DOI: 10.1080/15435075.2014.910776

Tomak, E. D., Ustaomer, D., Yildiz, S., and Pesman, E. (2014). "Changes in surface and mechanical properties of heat treated wood during natural weathering," *Measurement* 53, 30-39. DOI: 10.1016/j.measurement.2014.03.018

Tran, K.-Q., Luo, X., Seisenbaeva, G., and Jirjis, R. (2013). "Stump torrefaction for bioenergy application," *Applied Energy* 112, 539-546. DOI: 10.1016/j.apenergy.2012.12.053

Turner, I., Rousset, P., Rémond, R., and Perré, P. (2010). "An experimental and theoretical investigation of the thermal treatment of wood (*Fagus sylvatica* L.) in the range 200–260 °C," *International Journal of Heat and Mass Transfer* 53(4), 715-725. DOI: 10.1016/j.ijheatmasstransfer.2009.10.020

Uemura, Y., Omar, W., Othman, N. A., Yusup, S., and Tsutsui, T. (2013). "Torrefaction of oil palm EFB in the presence of oxygen," *Fuel* 103, 156-160. DOI: 10.1016/j.fuel.2011.11.018

Uemura, Y., Sellappah, V., Trinh, T. H., Hassan, S., and Tanoue, K.-I. (2017). "Torrefaction of empty fruit bunches under biomass combustion gas atmosphere," *Bioresource Technology* 243, 107-117. DOI: 10.1016/j.biortech.2017.06.057

Wang, S., Wang, K., Liu, Q., Gu, Y., Luo, Z., Cen, K., and Fransson, T. (2009). "Comparison of the pyrolysis behavior of lignins from different tree species," *Biotechnology Advances* 27(5), 562-567. DOI: 10.1016/j.biotechadv.2009.04.010

Werner, K., Pommer, L., and Broström, M. (2014). "Thermal decomposition of hemicelluloses," *Journal of Analytical and Applied Pyrolysis* 110, 130-137. DOI: 10.1016/j.jaap.2014.08.013

Xu, L., Yao, Q., Deng, J., Han, Z., Zhang, Y., Fu, Y., Huber, G. W., and Guo, Q. (2015). "Renewable N-heterocycles production by thermocatalytic conversion and ammonization of biomass over ZSM-5," *ACS Sustainable Chemistry & Engineering* 3(11), 2890-2899. DOI: 10.1021/acssuschemeng.5b00841

Xu, L., Yao, Q., Zhang, Y., and Fu, Y. (2017). "Integrated production of aromatic amines and N-doped carbon from lignin *via ex situ* catalytic fast pyrolysis in the presence of ammonia over zeolites," *ACS Sustainable Chemistry & Engineering* 5(4), 2960-2969. DOI: 10.1021/acssuschemeng.6b02542

Xu, J., Zhang, Y., Shen, Y., Li, C., Wang, Y., Ma, Z., and Sun, W. (2019). "New perspective on wood thermal modification: Relevance between the evolution of chemical structure and physical-mechanical properties, and online analysis of release of VOCs," *Polymers* 11(7), Article number 1145. DOI: 10.3390/polym11071145

Xue, Y., Zhou, S., and Bai, X. (2016). "Role of hydrogen transfer during catalytic copyrolysis of lignin and tetralin over HZSM-5 and HY zeolite catalysts," *ACS Sustainable Chemistry & Engineering* 4(8), 4237-4250. DOI: 10.1021/acssuschemeng.6b00733

Yin, C.-Y. (2011). "Prediction of higher heating values of biomass from proximate and ultimate analyses," *Fuel* 90(3), 1128-1132. DOI: 10.1016/j.fuel.2010.11.031

Zhen-Yu, W., Shu, Q., Zheng-Bin, H., Song-Lin, Y., and Jun, M. (2017). "Study of *Sabina chinensis* heartwood and sapwood pyrolysis with TG-FTIR analysis," *Spectroscopy and Spectral Analysis* 37(4), 1090-1094. DOI: 10.3964/j.issn.1000-0593(2017)04-1090-05

Zheng, A., Zhao, Z., Chang, S., Huang, Z., Wu, H., Wang, X., He, F., and Li, H. (2014). "Effect of crystal size of ZSM-5 on the aromatic yield and selectivity from catalytic fast pyrolysis of biomass," *Journal of Molecular Catalysis A: Chemical* 383, 23-30. DOI: 10.1016/j.molcata.2013.11.005

Article submitted: April 21, 2020; Peer review completed: May 31, 2020; Revised version received: June 26, 2020; Accepted: June 27, 2020; Published: July 2, 2020.
DOI: 10.15376/biores.15.3.6344-6370

APPENDIX

Supplementary Data

Table S1. Relative Content of Bio-oil Components from Pyrolysis of Raw and Torrefied Bamboo under Nitrogen

Category	Compounds	Relative Content (%)			
		Raw	BTN-200	BTN-250	BTN-
Acids	Acetic acid	2.76	4.32	2.83	2.69
	Palmitoleic acid	0.25	0.46	0.30	0.21
	Erucic acid	0.46	0.81	0.75	0.58
	Oleic acid	1.43	2.15	1.60	1.47
	3,5-Dimethoxy-4-hydroxyphenylacetic acid	0.66	0.23	0.29	0.54
	Pentadecanoic acid	0.51	0.91	0.56	0.64
	n-Hexadecanoic acid	5.05	5.94	4.00	3.12
	Octadecanoic acid	2.45	1.01	0.50	0.41
	Total	13.57	15.83	10.83	9.66
Phenols	Phenol	2.30	4.39	4.47	3.08
	Creosol	0.48	0.52	1.26	1.34
	Catechol	0.59	2.78	3.29	3.51
	4-Ethyl-phenol	5.05	5.24	7.67	8.52
	3-Methyl-phenol	6.01	6.22	7.69	8.01
	2,3,5-Trimethyl-phenol	0.30	0.47	0.78	1.06
	3-Ethyl-5-methyl-phenol	1.65	1.68	1.37	1.50
	4-Propyl-phenol	0.78	0.70	0.50	0.44
	2-Allylphenol	0.75	0.75	1.32	1.37
	2-Methoxy-4-vinylphenol	3.75	2.71	2.33	2.26
	2,6-Dimethoxy-phenol	4.95	5.04	6.60	8.54
	4-Ethylcatechol	1.68	1.70	1.69	1.56
	4-Methoxy-3-(methoxymethyl)-phenol	3.59	3.33	1.67	1.27
	(E)-4-(3-Hydroxyprop-1-en-1-yl)-2-	1.27	0.93	0.73	0.70
	(E)-2,6-Dimethoxy-4-(prop-1-en-1-yl)phenol	3.34	1.65	0.96	0.76
	Total	35.90	37.04	41.94	43.92
Furans	Furfural	3.13	2.83	2.47	1.25
	2,3-Dihydro-benzofuran	13.49	13.32	12.31	11.81
	Total	16.62	16.15	14.78	13.06
Ketones	3-Ethenyl-3-methylcyclopentanone	0.40	0.26	0.24	0.18
	1,2-Cyclopentanedione	1.38	1.23	0.89	0.89
	3-Methyl-1,2-cyclopentanedione	1.75	1.68	1.07	0.93
	3-Ethyl-2-hydroxy-2-cyclopenten-1-one	0.61	0.60	0.40	0.34
	Methandrostenolone	0.17	ND	ND	ND
	3,5-Dimethoxyacetophenone	3.58	2.51	1.55	0.90
	1-(4-Hydroxy-3,5-dimethoxyphenyl)-ethanone	0.80	0.78	0.75	0.67
	Total	8.69	7.06	4.90	3.91
Aldehydes	Heptanal	0.66	ND	ND	ND

	(E)-Cinnamaldehyde	0.25	0.23	0.21	0.18
	Vanillin	0.78	0.57	0.47	0.40
	4-Hydroxy-3,5-dimethoxy-benzaldehyde	0.75	0.61	0.25	0.23
	Total	2.44	1.41	0.93	0.81
Esters	7-Octynoic acid, methyl ester	0.37	0.44	0.55	0.61
	Hexanoic acid, 2-phenylethyl ester	0.73	0.87	1.56	1.95
	Formic acid, 2-(2-methoxyethyl)hexyl ester	0.61	0.61	0.66	0.79
	Methyl 5,7-hexadecadiynoate	0.47	0.48	1.00	0.66
	Diethyl phthalate	0.42	0.86	1.07	1.26
	Phthalic acid, isobutyl octadecyl ester	0.42	0.57	0.74	0.84
	Phthalic acid, butyl tetradecyl ester	1.20	1.44	1.85	1.87
	Total	4.22	5.27	7.43	7.98
Alcohol	4-Penten-1-ol	0.13	0.19	1.26	1.29
	4-Methyl-cyclohexanol	ND	ND	0.14	0.20
	3-Octyn-1-ol	1.33	0.64	0.25	0.21
	2,3-Dimethyl-cyclohexanol	0.32	0.31	0.21	0.24
	1-(1-Butyny)cyclopentanol	1.03	1.17	0.98	0.72
	6-Phenyl-5-hexyn-3-ol	0.88	0.89	0.51	0.45
	3-Methoxy-1,2-benzenediol	5.79	6.48	4.36	4.05
	Total	9.48	9.68	7.71	7.16
Hydrocarbon	Toluene	1.61	1.67	3.50	3.85
	o-Xylene	2.33	2.68	3.27	3.36
	1-Ethenyl-3-methyl-benzene	1.28	0.64	0.56	0.20
	D-Limonene	0.20	0.25	1.22	1.66
	3-Methyl-1H-indene	0.45	0.69	0.89	1.15
	Naphthalene	0.20	0.44	0.64	0.98
	Heptacosane	0.13	0.14	0.27	0.32
	Squalene	0.35	0.67	0.79	1.19
	Total	6.55	7.18	11.14	12.71
ND: Not detected					

Table S2. Relative Content of Bio-oil Components from Pyrolysis of BTO-200 under Different Oxygen Concentration

Category	Compounds	Relative Content (%)		
		BTO-200-3	BTO-200-6	BTO-200-
	Erucic acid	0.50	0.40	0.35
	Oleic acid	2.98	2.59	2.12
	Tetradecanoic acid	0.86	0.76	0.41
	3,5-Dimethoxy-4-hydroxyphenylacetic acid	0.56	0.49	0.15
	9-Hexadecenoic acid	0.55	0.54	0.37
	n-Hexadecanoic acid	6.77	5.58	5.58
	Octadecanoic acid	1.14	0.63	0.42
	Total	13.36	10.99	9.40
Phenols	Phenol	3.87	4.14	6.66
	Creosol	0.22	0.65	0.77
	Catechol	2.45	2.83	4.11
	4-Ethyl-phenol	2.49	2.91	3.76
	3-Methyl-phenol	1.29	3.09	3.73
	2-Allylphenol	0.25	0.56	1.39
	2-Methoxy-phenol	5.71	6.55	6.71
	2,4-Dimethyl-phenol	2.97	3.84	4.39
	3-Ethyl-5-methyl-phenol	1.14	1.21	2.52
	2,5-Dimethyl-phenol	0.40	0.61	1.72
	3-Methoxy-5-methylphenol	2.10	2.19	2.40
	2,6-Dimethoxy-phenol	2.30	2.95	3.33
	2-Methoxy-4-propyl-phenol	3.82	4.73	5.15
	4-Methoxy-3-(methoxymethyl)- phenol	6.57	4.30	l.97
	(E)-2,6-Dimethoxy-4-(prop-1-en-1-yl)phenol	2.07	1.32	0.51
	Total	37.65	41.88	49.12
Furans	Furan, 2,5-dimethyl-	2.96	1.69	1.21
	Benzofuran, 2-methyl-	0.51	0.29	ND
	Benzofuran, 2,3-dihydro-	9.73	9.00	5.03
	Total	12.69	10.98	6.24
Ketones	3-Ethenyl-3-methylcyclopentanone	0.41	0.29	0.24
	1,2-Cyclopentanedione	1.52	1.30	0.69
	3-Methyl-1,2-cyclopentanedione	1.60	1.42	1.18
	2,3-Dimethyl-2-cyclopenten-1-one	1.10	0.86	0.42
	1-(4-Hydroxy-3,5-dimethoxyphenyl)-ethanone	0.66	0.52	0.24
	Total	5.29	4.39	2.77
Aldehydes	2-Ethyl-2-hexenal	0.57	0.52	0.18
	(E)-2-Dodecenal	0.22	0.18	0.13
	4-Hydroxy-3,5-dimethoxy-benzaldehyde	0.45	0.42	0.30
	Total	1.24	1.12	0.61
Esters	7-Nonenoic acid, methyl ester	0.43	0.58	0.58
	Benzenepropanoic acid, 10-undecenyl ester	0.57	1.06	2.31
	Glutaric acid, di(isobutyl) ester	0.38	0.53	0.64
	Diethyl phthalate	0.53	0.68	0.72

	Phthalic acid, isobutyl octadecyl ester	1.38	1.43	1.49
	Octadecanoic acid, 4-hydroxy-, methyl ester	0.10	0.14	0.18
	Hexadecanoic acid, 14-methyl-, methyl ester	0.09	0.21	0.37
	Total	3.48	4.63	6.29
Alcohol	4-Penten-1-ol	1.62	1.66	1.66
	(Z)-3-Hexen-1-ol	1.26	1.20	0.53
	4-Methyl-cyclohexanol	0.13	0.26	0.31
	2-Furanmethanol	1.66	1.43	0.88
	4-Methyl-1,2-benzenediol	2.37	1.12	1.10
	2,5-Dimethyl-1,4-benzenediol	0.74	1.23	0.86
	2,3-Dimethyl-cyclohexanol	4.77	3.98	1.43
	Total	12.55	10.88	6.77
Hydrocarbon	Benzene	ND	ND	0.75
	Toluene	3.68	3.83	4.02
	o-Xylene	1.73	1.79	3.07
	D-Limonene	1.05	1.87	2.48
	Naphthalene	1.32	1.32	1.36
	1-Ethyl-3-methyl-benzene	0.43	1.00	1.81
	3-Methyl-1H-indene	0.31	0.66	1.11
	Heptacosane	0.55	1.00	1.13
	2-Hexadecanol	0.08	0.10	0.12
	Squalene	0.57	0.68	0.90
	Total	9.72	12.25	16.75
ND: Not detected				

Table S3. Relative Content of Bio-oil Components from Pyrolysis of BTO-250 under Different Oxygen Concentration

Category	Compounds	Relative Content (%)		
		BTO-250-3	BTO-250-6	BTO-250-
Acids	Oleic acid	2.13	1.92	1.66
	Erucic acid	1.47	1.44	0.97
	Tetradecanoic acid	0.88	0.66	0.51
	3,5-Dimethoxy-4-hydroxyphenylacetic acid	0.42	0.38	0.22
	9-Hexadecenoic acid	0.32	0.18	0.13
	n-Hexadecanoic acid	3.02	3.26	3.53
	Octadecanoic acid	1.08	1.02	0.90
	Total	9.32	8.86	7.92
Phenols	Phenol	4.18	5.32	7.77
	Creosol	0.43	0.79	1.01
	Catechol	2.86	3.12	4.88
	p-Cresol	4.86	6.02	8.66
	3-Methyl-phenol	1.33	3.02	3.63
	2-Allylphenol	0.48	0.77	1.41
	2,4-Dimethyl-phenol	4.87	3.32	1.99
	2-Methoxy-phenol	6.82	6.93	7.32
	2,5-Dimethyl-phenol	0.31	0.44	0.58
	2,6-Dimethoxy-phenol	2.18	2.86	3.03
	4-Ethyl-2-methoxy-phenol	2.38	1.94	1.28
	4-Methoxy-3-(methoxymethyl)-phenol	9.09	7.36	5.34
	(E)-2,6-Dimethoxy-4-(prop-1-en-1-yl)phenol	4.03	3.28	2.19
	Total	43.82	45.17	49.18
Furans	2,5-dimethyl-Furan	1.36	0.84	0.74
	2,3-dihydro-Benzofuran	8.32	6.55	4.38
	Total	9.68	7.39	5.12
Ketones	3-Ethenyl-3-methylcyclopentanone	0.34	0.28	0.19
	1,2-Cyclopentanedione	1.28	1.15	0.43
	3-Methyl-1,2-cyclopentanedione	0.79	0.61	0.29
	2,3-Dimethyl-2-cyclopenten-1-one	0.30	0.46	0.36
	1-(1-Cyclohexen-1-yl)-ethanone	0.33	0.21	0.17
	2-[2-(2-Butoxyethoxy)ethoxy]-ethanol	0.34	0.41	0.43
	Total	3.38	3.12	1.87
Aldehydes	2-Ethyl-2-hexenal	0.33	0.26	0.20
	(E)-2-Dodecenal	0.22	0.18	0.17
	3-[4-(1,1-Dimethylethyl)phenoxy]-benzaldehyde	0.34	0.33	0.34
	Total	0.89	0.77	0.71
Esters	Hexanoic acid, 2-phenylethyl ester	0.56	0.99	1.55
	Glutaric acid, di(isobutyl) ester	0.73	0.82	0.96
	Diethyl phthalate	2.55	1.19	0.98
	Hexadecanoic acid, methyl ester	1.01	1.28	1.76
	Phthalic acid, butyl tetradecyl ester	2.97	3.86	4.51
	Octadecanoic acid, 4-hydroxy-, methyl ester	0.30	0.47	0.68

	Total	8.12	9.38	10.44
Alcohol	4-Penten-1-ol	1.78	1.83	1.89
	2-Methyl-benzene methanol	0.44	0.32	0.18
	2-Furanmethanol	2.97	2.71	1.80
	3-Methoxy-1,2-benzenediol	3.21	1.03	0.35
	2,5-Dimethyl-1,4-benzenediol	0.63	0.31	0.21
	2,3-Dimethyl-cyclohexanol	0.26	0.16	0.09
	Total	9.29	6.36	4.52
Hydrocarbon	Benzene	1.38	1.44	1.68
	Toluene	3.92	4.27	4.44
	o-Xylene	1.78	1.90	2.03
	D-Limonene	3.32	3.47	3.71
	1,2-Dihydro-3-methyl-naphthalene	0.32	0.39	0.48
	Heptacosane	0.86	1.66	1.66
	2-Hexadecanol	0.19	0.33	0.46
	Squalene	1.61	3.53	3.86
	Total	13.38	16.99	18.32
ND: Not detected				

Table S4. Relative Content of Bio-oil Components from Pyrolysis of BTO-300 under Different Oxygen Concentration

Category	Compounds	Relative Content (%)		
		BTO-300-3	BTO-300-6	BTO-300-
Acids	Palmitoleic acid	1.01	1.14	1.24
	Erucic acid	0.68	1.40	1.43
	Oleic acid	1.48	1.57	1.91
	Tetradecanoic acid	0.83	1.36	1.62
	Pentadecanoic acid	0.59	0.82	1.40
	9-Hexadecenoic acid	0.79	0.83	1.20
	n-Hexadecanoic acid	5.71	5.98	6.51
	Total	11.09	13.10	15.31
Phenols	Phenol	3.21	3.43	5.11
	Creosol	2.66	2.74	2.76
	Catechol	1.14	1.33	2.41
	m-Guaiacol	0.20	0.26	0.37
	p-Cresol	1.36	3.57	6.13
	3-Methyl-phenol	1.68	0.43	0.27
	2,5-Dimethyl-phenol	1.28	0.61	0.19
	2-Methoxy-phenol	5.42	4.02	2.95
	2,4-Dimethyl-phenol	1.53	0.56	0.47
	4-Ethyl-phenol	2.45	1.94	1.56
	4-Ethyl-2-methoxy-phenol	1.92	1.69	1.38
	2,6-Dimethoxy-phenol	10.88	8.55	7.38
	4-Methoxy-3-(methoxymethyl)-phenol	2.23	1.19	0.88
	3-(1,1-Dimethylethyl)-4-methoxy-phenol	4.15	3.47	2.37
	2,6-Dimethoxy-4-(2-propenyl)-phenol	1.94	1.13	0.94
	Total	42.05	34.92	33.79
Furans	2,5-Dimethyl-furan	1.04	0.82	0.24
	2,3-Dihydro-benzofuran	2.55	1.92	1.85
	Total	3.59	2.74	2.09
Ketones	3-Ethenyl-3-methylcyclopentanone	0.29	0.20	0.19
	4-Ethyl-4-methyl-2-cyclohexen-1-one	0.58	0.43	0.40
	2,3-Dimethyl-2-cyclopenten-1-one	0.33	0.28	0.13
	1-(1-Cyclohexen-1-yl)-ethanone	0.40	0.30	0.26
	4-Methyl-5-(2-methyl-2-propenyl)-2(5H)-	0.35	0.26	0.20
	2-[2-(2-Butoxyethoxy)ethoxy]-ethanol	0.70	0.60	0.26
	Total	2.65	2.07	1.44
Aldehydes	(Z)-9-Tetradecenal	0.14	ND	ND
	(E)-2-Dodecena	0.18	0.25	0.14
	3-[4-(1,1-Dimethylethyl)phenoxy]-benzaldehyde	0.71	0.27	0.25
	Total	1.03	0.52	0.39
Esters	Hexanoic acid, 2-phenylethyl ester	0.43	0.63	0.95
	2,5-Octadecadiynoic acid, methyl ester	0.52	0.65	0.74
	Isobornyl acetate	0.09	0.13	0.30
	Diethyl phthalate	1.62	2.50	2.69

	Geranyl isovalerate	0.14	0.20	0.32
	Glutaric acid, di(isobutyl) ester	0.52	1.23	2.17
	Hexadecanoic acid, methyl ester	0.71	1.36	1.73
	Phthalic acid, butyl tetradecyl ester	3.13	4.28	4.52
	Heptadecanoic acid, 16-methyl-, methyl ester	1.21	1.99	2.40
	Oleic acid, 3-(octadecyloxy)propyl ester	0.20	0.22	0.43
	Total	8.57	13.19	16.25
Alcohol	4-Penten-1-ol	2.84	2.34	1.93
	2-Methyl-benzenemethanol	0.68	0.23	0.21
	3-Methoxy-1,2-benzenediol	5.90	5.14	1.03
	2,5-Dimethyl-1,4-benzenediol	0.67	0.36	0.19
	2-Methyl-1-hexadecanol	1.59	1.30	1.21
	4-Hydroxy-benzenemethanol	0.26	ND	ND
	α-Ethyl-4-methoxy-benzenemethanol	0.32	0.21	0.16
	Total	12.26	9.58	4.73
Hydrocarbon	Toluene	1.23	1.23	1.47
	1,3-Dimethyl-benzene	0.10	0.14	0.19
	p-Xylene	0.72	0.82	1.25
	D-Limonene	7.01	9.57	9.83
	1,2-Dihydro-3-methyl-naphthalene	0.50	0.80	1.35
	3,5-Dimethoxy-4-hydroxytoluene	1.00	1.45	1.47
	Naphthalene	2.17	2.38	2.41
	Heptacosane	1.10	1.43	2.32
	Squalene	1.94	2.76	3.84
	Total	15.77	20.58	24.13
ND: Not detected				